A Conserved Role for Vezatin Proteins in Cargo-Specific Regulation of Retrograde Axonal Transport

Michael A. Spinner,* Katherine Pinter,† Catherine M. Drerup,† and Tory G. Herman*,1

*Institute of Molecular Biology, University of Oregon, Eugene, Oregon 97403 and †Unit on Neuronal Cell Biology, National Institute of Child Health and Human Development, National Institutes of Health, Bethesda, Maryland 20892

ABSTRACT Active transport of organelles within axons is critical for neuronal health. Retrograde axonal transport, in particular, relays neurotrophic signals received by axon terminals to the nucleus and circulates new material among *en passant* synapses. A single motor protein complex, cytoplasmic dynein, is responsible for nearly all retrograde transport within axons: its linkage to and transport of diverse cargos is achieved by cargo-specific regulators. Here, we identify Vezatin as a conserved regulator of retrograde axonal transport. Vertebrate Vezatin (Vezt) is required for the maturation and maintenance of cell-cell junctions and has not previously been implicated in axonal transport. However, a related fungal protein, VezA, has been shown to regulate retrograde transport of endosomes in hyphae. In a forward genetic screen, we identified a loss-of-function mutation in the *Drosophila vezatin-like* (*vezl*) gene. We here show that *vezl* loss prevents a subset of endosomes, including signaling endosomes containing activated BMP receptors, from initiating transport out of motor neuron terminal boutons. *vezl* loss also decreases the transport of endosomes and dense core vesicles, but not mitochondria, within axon shafts. We disrupted *vezt* in zebrafish and found that *vezt* loss specifically impairs the retrograde axonal transport of late endosomes, causing their accumulation in axon terminals. Our work establishes a conserved, cargo-specific role for Vezatin proteins in retrograde axonal transport.

KEYWORDS Vezatin; Diamond; axonal transport; retrograde; endosome

NEURONS mediate cognition and behavior by forming networks that can have complex connectivity and span considerable distances. As a consequence, neurons have elongated processes along which passive diffusion is inefficient and materials must be actively transported [recently reviewed in Guedes-Dias and Holzbaur (2019)]. Within axons, cargoes move along uniformly polarized microtubules by binding to active kinesin or cytoplasmic dynein motors: the former move associated cargo in the anterograde direction, toward microtubule plus ends and the axon terminal, and the latter move cargo in the retrograde direction, back to the soma (Guedes-Dias and Holzbaur 2019). Bidirectional axonal transport is essential for the function and survival of neurons, and abnormalities in this process are an early hallmark of neurodegenerative diseases such as Huntington's, Alzheimer's, and Parkinson's diseases (Guo *et al.* 2020).

How axonal transport is regulated remains a central question. While multiple kinesin family members transport the cargos that move toward axon terminals, the majority of retrograde axonal transport is accomplished by a single motor protein complex, cytoplasmic dynein. Dynein's ability to bind cargo and microtubules is enhanced by its cofactor, dynactin. However, a variety of cargo-specific regulators are additionally required: some link cargoes to dynein-dynactin complexes, some promote the motility of cargo-bound dynein-dynactin, and some do both (Reck-Peterson *et al.* 2018). While many such regulators have been identified, others undoubtedly remain to be discovered.

The *Drosophila* larval neuromuscular junction (NMJ) is well-suited to the identification and analysis of genes required for axonal transport (Neisch *et al.* 2016). Each motor neuron forms a stereotyped pattern of branched chains of synaptic boutons on its target muscle and adds new boutons in response to a muscle-secreted Bone Morphogenetic Protein (BMP) signal during larval growth [reviewed in Deshpande and Rodal (2016)]. Within larval motor neuron

axons, two broad types of cargoes are retrogradely transported: (1) those (such as signaling endosomes containing activated BMP receptors) that originate in the boutons themselves and are transported through the NMJ and axon shaft to the soma [Lloyd *et al.* 2012; Smith *et al.* 2012]; and (2) those (such as dense core vesicles (DCVs)] that originate in the soma and are anterogradely transported to the terminal boutons of each NMJ, but require retrograde transport within the NMJ itself to be distributed among the other *en passant* boutons (Wong *et al.* 2012). Both types of cargo accumulate in terminal boutons when dynactin is disrupted by loss of its core subunit p150[Glued] (Lloyd *et al.* 2012).

Forward genetic screens in invertebrates continue to uncover new relationships between molecules and phenotypes. In such a screen, we identified a loss-of-function mutation in the *Drosophila* gene, *diamond* (Graziadio *et al.* 2018), that results in enlarged terminal boutons containing accumulated retrograde cargos. We found that the predicted Diamond protein is most closely related to vertebrate Vezatin (Vezt) in amino acid sequence and, on that basis, will refer to the *Drosophila* gene as *vezatin-like* (*vezl*). Vertebrate Vezt was originally identified as an adherens junction-associated protein that links cadherin-catenin complexes to the FERM domain-containing proteins myosin VIIa (Küssel-Andermann *et al.* 2000) and radixin (Bahloul *et al.* 2009). Vezt has subsequently been found postsynaptically in both muscle and dendrites and is required for the maturation and maintenance of adherens junctions (Hyenne *et al.* 2005; Hyenne *et al.* 2007), dendrites (Sanda *et al.* 2010; Danglot *et al.* 2012), and NMJ synapses (Koppel *et al.* 2019). A forward genetic screen in *Aspergillus* identified a Vezt-like *Aspergillus* protein, VezA, as being required for dynein-dependent transport of endosomes in hyphae (Yao *et al.* 2015). Here, we show that both fly *vezl* and zebrafish *vezt* are required for the retrograde transport of late endosomes in axons. Our data identify a conserved role for Vezt proteins as cargo-specific regulators of retrograde axonal transport.

Materials and Methods

Drosophila genetics

Flies were grown on standard food at 25°. The *721* mutation was the result of exposing wild-type *FRT82*-containing flies [Bloomington *Drosophila* Stock Center (BDSC) stock no. 1359] to ethylmethane sulfonate using standard methods (Ashburner 1989). The *vezl[13.1]* deletion was generated by imprecise excision of a *white[+] P* element within exon 1 (BDSC stock no. 31820). Briefly, *white[−]* lines generated by mobilizing the *P* element were tested for their ability to complement *721* for lethality. DNA from those that failed to complement *721* was sequenced with primers flanking the *CG7705* gene region. The *13.1* deletion removed most of *CG7705* without extending beyond it. Homozygous wild-type (*FRT82*), *FRT82 vezl[721]*, or *FRT82 vezl[13.1]* R7s were created by *GMR-FLP*-induced mitotic recombination (Lee *et al.* 2001) and labeled by the Mosaic

analysis with a repressible cell marker (MARCM) technique (Lee and Luo 1999), using *actin-Gal4* to drive *UAS-synaptotagmin-GFP*. *Df(3R)Exel6180* (BDSC stock no. 7659) is a molecularly defined deletion that completely removes *vezl* along with 23 other genes; *vezl[13.1]/Df(3R)Exel6180* homozygous larvae are viable as late third instar larvae, but die either shortly before or after pupariation. All NMJ analyses were performed using motile third instar larvae responsive to touch.

The *UAS-Vezl[wt]:Venus* and *UAS-hVez:Venus* transgenes were generated by cloning a full-length *vezl* complementary DNA (cDNA) (LP22035; obtained from the Berkeley *Drosophila* Genome Project) or a full-length human *vezatin* cDNA (BC064939; obtained from Dharmacon) into pUAST vectors containing a C-terminal Venus open reading frame (Wang *et al.* 2012; Addgene plasmid no. 35204). Transgenes were sequenced and then injected into embryos containing an attP8 site on the *X* chromosome (BDSC stock no. 32233; BestGene).

Flies containing *UAS-Tkv:mCherry* were a generous gift from Thomas Kornberg (Roy *et al.* 2014). Stocks containing all other transgenes used were obtained from BDSC: *actin-Gal4* (stock no. 4414), *UAS-synaptotagmin:GFP* (stock no. 6525), *OK371-Gal4* (stock no. 26160), *UAS-ANF:GFP* (stock no. 7001), *UAS-YFP:Rab5* (stock no. 50788), *UAS-Rab7:GFP* (stock no. 42705), *UAS-Rab11:GFP* (stock no. 8506), and *UAS-mito:GFP* (stock no. 8442). Because many transgenes used were located on the *X* chromosome, we analyzed females only, for consistency.

Sequence alignment and domain prediction

The third iteration of Position-Specific Iterative (PSI)-BLAST (https://blast.ncbi.nlm.nih.gov/) identified vertebrate Vezts as having sequence similarity to Vezl. Sequence alignments in Figure 1H were performed with ClustalW2 (Geneious). Supplemental Material, Figure S1 shows the sequence alignment between Vezl and human Vezt (hVezt) that was generated by PSI-BLAST, as well as the alignment with the pfam12632 "Vezatin domain" consensus sequence. Domains indicated in Figure 1H were predicted using InterPro (https://www.ebi.ac.uk/interpro/), SMART (http://smart.embl-heidelberg.de/), or PrDOS (http://prdos.hgc.jp/cgi-bin/top.cgi).

Drosophila dissections, fixation, and immunostaining

Adult brains were dissected and fixed in 4% paraformaldehyde at room temperature for 20 min. Late third instar larval NMJs were dissected in Schneider's insect medium (Sigma-Aldrich, St. Louis, MO) and fixed with Bouin's solution (Sigma-Aldrich) for 5 min. All samples were then stained by standard methods: washed three times in PBS containing 0.3% Triton-X 100 (PBT), blocked for 30 min in 5% normal goat serum, incubated with primary antibodies at 4° overnight, washed three times with PBT, incubated with secondary antibodies at 4° overnight, washed three times with PBT, and mounted in Vectashield (Vector Laboratories). We used the following primary antibodies from the Developmental Studies Hybridoma Bank: anti-Chp (24B10, at dilution 1:200), anti-Discs large (Dlg) (4F3, at dilution 1:250), anti- Cysteine

String Protein (CSP) (6D6, at dilution 1:250), and anti-Bruchpilot (Brp) (nc82, at dilution 1:100). Other primary antibodies used were rabbit anti-GFP (1:1000; Abcam), fluorescence-conjugated anti-HRP (1:250; Jackson ImmunoResearch Laboratories), rabbit anti-GFP (1:1000; Abcam), rabbit anti-pMad (1:500, a gift from Carl Heldin; Persson *et al.* 1998), and rabbit anti-GluRIIC (1:2500, a gift from Aaron DiAntonio; Marrus *et al.* 2004). All secondary antibodies were goat IgG coupled with Alexa Fluor 488, 555, or 633 (1:500; Thermo Fisher Scientific). As noted in the Figure 6A legend, Vezl:Venus was imaged by dissecting but not fixing late third instar larvae; fluorescence-conjugated anti-HRP was added to the dissection media.

Quantification of Drosophila R7 and NMJ morphology in fixed samples

For all comparative experiments, animals from each genotype were grown, dissected, and stained in parallel and imaged on the same day under identical microscope settings. Z-sections were collected on a Leica SP2 microscope (with a $\times63$/NA 1.4 oil objective). For Figure S2, C–E, structured illumination microscopy (SIM) images were collected using a Zeiss ELYRA S.1/LSM 880 confocal microscope with a Plan-Apochromat $\times63$/NA 1.4 oil objective (Zeiss, Thornwood, NY). Within each experiment, the images were randomized, and quantifications were performed blind to genotype. For Figure 1E, ~100 R7 axons were scored within each animal to determine the percentage of R7s with terminal blobs for that animal. For Figures 2–4 and Figures S2 and S3, maximum-intensity projections of z-stacks were generated and analyzed with ImageJ software (Schindelin *et al.* 2012; http://fiji.sc/). As is standard (*e.g.*, Ball *et al.* 2010), we counted boutons based on shape, as visualized by anti-HRP and anti-Dlg staining on muscle 4 on both sides of segment A3, and calculated the mean for each animal. Satellite boutons were identified as smaller, nonchain-forming, individual boutons that emerged from larger boutons on the main NMJ axis (*e.g.*, Marie *et al.* 2004); they were counted separately and not included in total NMJ bouton counts. The relative sizes and staining intensities of terminal boutons were measured in ImageJ by manually tracing each terminal bouton and its immediate neighbors. Each z-stack in which intensities were quantified consisted of only three to five z-sections (boutons are shallow), with little variation in intensity at a given xy position within the stack except at positions that were outside the bouton in a subset of slices; maximum-intensity projections therefore provided an accurate assessment of the accumulation of signal within terminal relative to nonterminal boutons.

Drosophila live imaging and analysis

Wandering late third instar larvae were dissected to expose the area of interest in Ca^{2+}-free HL3 media on a custom-made Sylgard mount, secured with a coverslip, and immediately imaged in a temperature-controlled room during similar times of day. Live imaging within single planes was conducted using a Zeiss ELYRA S.1/LSM 880 (with

a Plan-Apochromat $\times63$/NA 1.4 oil objective) with the pinhole set at >1 Airy Unit to optimize the ability to monitor individual particles. Videos were recorded with a minimum of two frames per second over the course of 6–10 min time spans to ensure the larvae did not die during imaging. Movement of individual Tkv:mCherry puncta within NMJ boutons (Figure 5) was trackable without the use of fluorescence recovery after photobleaching (FRAP). However, we did use FRAP to track individual ANF:GFP puncta movement within NMJ boutons: we bleached a region of interest adjacent to the terminal bouton with a 488-nm laser for 60 sec at high power, followed by regular image acquisition. In all cases, the number of puncta that entered or left the terminal bouton over the movie's time span was counted manually. Imaging of ANF:GFP, Tkv:mCherry, and mito:GFP movement within axons was performed in individual axon bundles, near the ventral nerve cord. Velocities were calculated based on the slopes of kymographs generated by the Multi kymograph tool in ImageJ. Puncta were counted and then watched for directional movement over a fixed timeframe of 3–5 min to categorize them as stationary, anterograde-moving, or retrograde-moving. These numbers were normalized to the area of the region being imaged.

Zebrafish husbandry and generation of the vezt mutant line

Adult zebrafish were housed at $28°$ and bred using established protocols (Westerfield 1993) in accordance with The National Institute of Child Health and Human Development/International Animal Care and Use Committee/IACUC protocol Drerup 18.008. Embryos and larvae were housed at $28°$ in embryo media and staged by established methods (Kimmel *et al.* 1995). The *TgBAC(neurod:egfp)[nl1]* transgenic line was used to label neurons with cytoplasmic GFP (Obholzer *et al.* 2008).

The *vezt[y624]* mutant line was generated using CRISPR/Cas9 mutagenesis (Burger *et al.* 2016). Briefly, 500 ng Cas9 protein (Integrated DNA Technologies) was co-injected with ~200 pg guide RNA targeted against exon three of the zebrafish *vezt* ortholog (GTGGCGCTGTCTCGACGCAG). Resulting F_0 animals were raised and crossed to wild-type animals to generate F_1 larvae. Sequencing of the F_1 larvae revealed an F_0 carrier of a 5-bp insertion in exon three of *vezt*, predicted to cause the insertion of 40 amino acids followed by a premature stop site. Fragment length analysis of PCR products flanking this region were used to genotype (Carrington *et al.* 2015). The *vezt[y624]* mutation is homozygous lethal, and the axon terminal swelling phenotype it causes is recessive.

Immunolabeling and fluorescence intensity quantification in zebrafish

Homozygous embryos were generated by *vezt[y624]* heterozygous crosses. Larvae were raised to 4 days postfertilization (dpf), fixed in 4% paraformaldehyde, and stained as in Drerup and Nechiporuk (2013). Antibodies used were anti-Dync1h1 (#12345; Proteintech), anti-p150 (#610473; BD Transduction Laboratories), anti-Cytochrome C (#556432; BD Pharmaceutical Systems), anti-GFP (#gfp-1020; Aves

Labs), and Alexa Fluor 488/568 secondaries (Thermo Fisher Scientific).

After immunolabeling, larvae were imaged on a Zeiss LSM 800 confocal microscope with a ×63/NA 1.4 oil objective. Optical sections were obtained at ∼0.5 μm intervals spanning the full depth of the axon terminal. For quantification of immunofluorescence, a custom ImageJ macro was used to isolate the fluorescence signal from the GFP-labeled axons. A summed projection was generated and then the mean fluorescence intensity was quantified. Mean fluorescence was normalized to background. Statistical analyses were done in JMP.

In vivo analysis of axon terminal volume and endosome localization and transport in zebrafish

To determine axon terminal volumes, axon terminals were imaged using an LSM800 confocal microscope with a ×63/NA 1.2 water immersion objective and identified using the GFP axon fill from the *TgBAC(neurod:egfp)^{nl1}* transgene. Axon terminal volumes were calculated in ImageJ using the three-dimensional object counter plugin.

Larvae mosaically expressing endosome markers were generated as previously described (Drerup and Nechiporuk 2013). Briefly, zygotes were microinjected with DNA plasmids encoding a neuron-specific promoter (*5kbneurod*) driving expression of the particular Rab fused to mRFP. Larvae expressing the construct of interest in posterior lateral line (pLL) sensory neurons were isolated using an AxioZoom fluorescence dissecting microscope, mounted in 1.5% low melt agarose, and imaged on a LSM800 confocal microscope using a ×63/NA 1.2 water immersion objective (Zeiss). For analyses of Rab5/7/11 vesicle localization, *z*-sections were obtained through each expressing pLL axon terminal. An SD projection was then done in ImageJ and the total particle area was quantified. The axon terminal area was also measured and the number of axon terminals recorded so that the endosome area could be normalized to axon terminal area or to axon number, to account for the mosaicism of the Rab labeling and the increased axon terminal volume in *vezt^{y624}* mutants.

For analyses of vesicle transport, larvae were mounted similarly and imaged with the LSM800 confocal using the ×63/NA 1.2 water immersion objective (Zeiss), as previously described (Drerup and Nechiporuk 2016). Images were taken three times per second for 150 sec, over a region of pLL axon in a single plane to track the location of moving puncta. Imaging sessions were analyzed using Kymograph analysis in Metamorph (Molecular Devices). Transport distance was quantified and statistical significance was analyzed using JMP.

Experimental design, statistical analyses, and data availability

All experiments were scored blind to genotype. For comparisons in Figures 1–6 and Figures S2 and S3, one-way ANOVA was performed, followed by select *post hoc* comparisons using two-tailed *t*-tests; for multiple comparisons (Figures 1E and Figure 2, I–L), Bonferroni-corrected *P*-values were used. For comparisons in Figure 7 and Figure S4, two-way ANOVA

was performed. The means, *n* values, SEMs, *P*-values, and Bonferroni-corrected *P*-values presented in the bar graphs are available in Table S1. All specifics of the data are available upon request, as are DNA constructs and fly and fish stocks. Supplemental material available at figshare: https://doi.org/10.25386/genetics.12780461.

Results

Loss of a Vezl protein alters the morphology of terminal synaptic boutons in adult eye and at the larval NMJ

Drosophila R7 photoreceptor neurons are a convenient cell type with which to identify essential genes that are required cell-autonomously for neuronal function. Photoreceptors are not required for viability, and the *GMR-FLP*/MARCM technique can be used to generate mosaic animals in which Green Fluorescent Protein (GFP)-labeled R7s are homozygous for randomly mutagenized chromosome arms within otherwise heterozygous animals (Lee and Luo 1999; Lee *et al.* 2001). In a screen of ethylmethane sulfonate-induced mutations, we identified a mutation, *721*, that alters R7 synaptic bouton morphology. Both wild-type and *721* mutant R7 axons terminate in ellipsoid boutons within the M6 layer of the optic lobe (Figure 1, A and B). However, *721* mutant R7 terminals also frequently extend short, thin projections that end in distinctive blobs beyond M6 (Figure 1, A and B).

Animals homozygous for the *721*-containing chromosome do not survive to adulthood. Using recombination mapping and complementation tests between the *721*-containing chromosome and molecularly-defined deletions, we found that both the lethality and the R7 defect are linked to a gene, *CG7705*, recently renamed "*diamond*" (Graziadio *et al.* 2018). The predicted CG7705/Diamond protein has no obvious sequence motifs, and simple BLAST searches identify homologs only in other Drosophilid species. However, PSI-BLAST identifies a similarity between CG7705/Diamond and vertebrate Vezt proteins (Figure 1, F and H and Figure S1; Küssel-Andermann *et al.* 2000). For this reason, and because of the shared function we describe later in this paper, we will refer to CG7705/Diamond as Vezl. Despite a low percentage of amino acid sequence identity in any pairwise comparison (Figure 1F), Vezl, Vezt, and the related fungal protein VezA share a predicted overall structure, consisting of central alpha-helical transmembrane domains and N- and C-terminal disordered regions (Figure 1H). We note that a so-called "Vezatin domain," which, in vertebrate Vezt, binds the FERM domains of myosin VIIa and radixin (Küssel-Andermann *et al.* 2000; Bahloul *et al.* 2009), is not detected by an InterPro scan of Vezl (Figure 1H, Figure S1).

To verify that *vezl* loss is responsible for the R7 blobs, we used imprecise excision of a previously identified *P*-element insertion within the first exon of *vezl* to generate a deletion allele, *vezl^{13.1}*, that is missing most of the predicted *vezl* open reading frame (Figure 1G). *vezl^{13.1}* homozygotes die either shortly before or after pupariation, and homozygous *vezl^{13.1}* mutant R7 terminal boutons within heterozygous animals
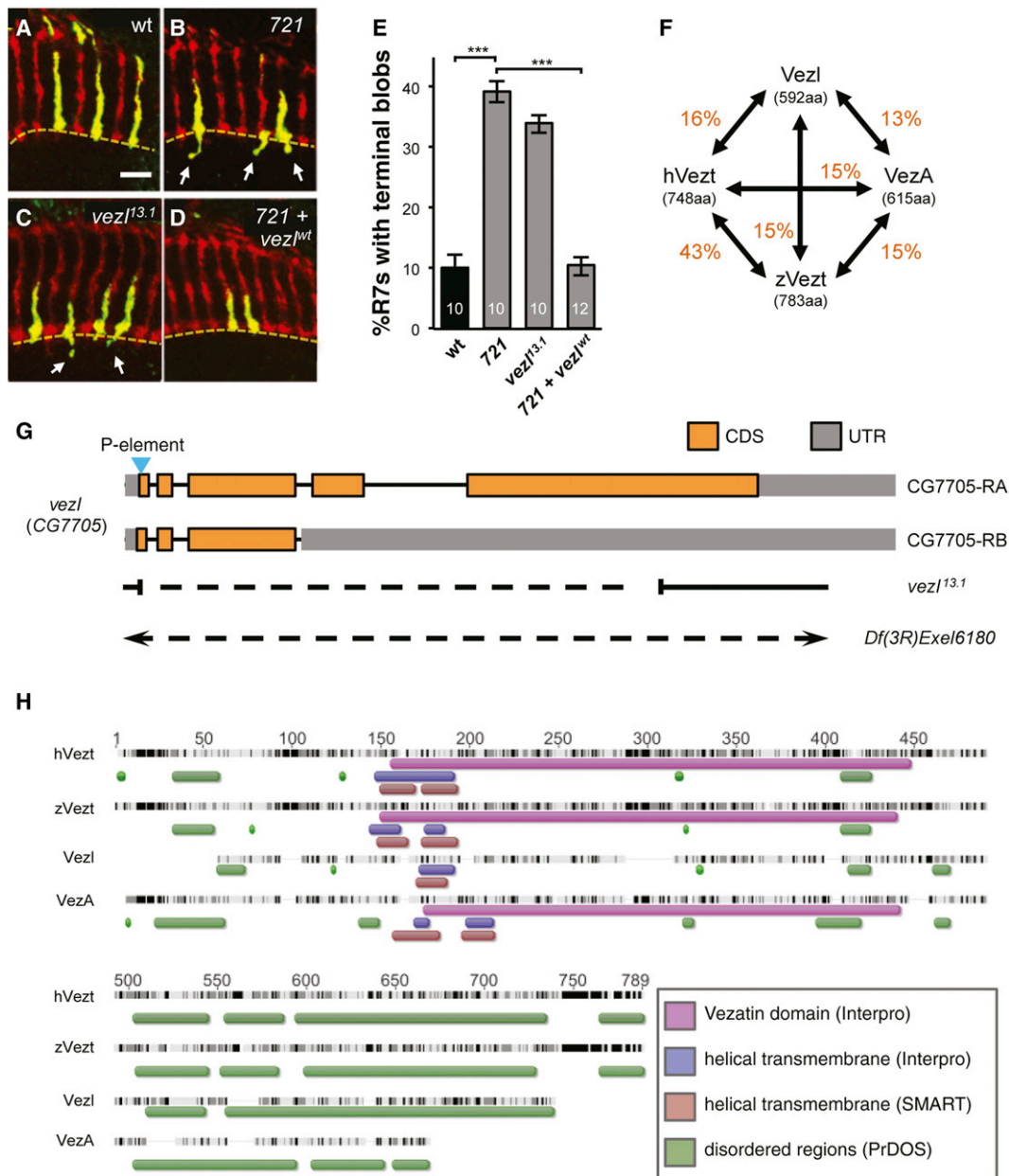
Figure 1 Vezl is required in R7 photoreceptors for normal axon terminal morphology. (A–D) Adult medullas in which homozygous R7s generated by *GMR-FLP*/MARCM express Synaptotagmin:GFP (green). All R7 and R8 axons are labeled with anti-Chaoptin (Chp; red). The M6 layer of the medulla is indicated by a dashed yellow line. Bar, 10 μm. (A) Wild-type (homozygous *FRT82*) R7 axons terminate in ellipsoid synaptic boutons in M6. (B) The axon terminals of R7s homozygous for the *721* mutation are ellipsoid but frequently have short extensions that end in blobs (arrows) beyond M6. (C) R7s homozygous for *13.1*, which deletes most of the *CG7705*/*vezl* open reading frame (see G), have the same axon terminal defect as *721* homozygous R7s (arrows point to terminal blobs). (D) Expression of a *vezl* cDNA in *721* homozygous R7s fully rescues their axon terminal defect. (E) Quantification of ectopic terminal blobs in A–D genotypes. The percentage of R7s with terminal blobs was calculated for each animal. The number of animals is indicated on each bar. Error bars indicate SEM. *** $P < 0.001$, based on two-tailed *t*-tests with Bonferroni correction. Means, SEMs, and *P*-values are available in Table S1. (F) Amino acid sequence comparisons among fly Vezl, human Vezatin (hVez), *A. nidulans* VezA, and zebrafish Vezatin (zVez). Each value in orange indicates the percentage of amino acid identity between a given pair. (G) Diagram showing the approximate breakpoints of the *vezl13.1* deletion relative to the locations of the *vezl* exons found in the two types of *vezl* mRNA identified, "CG7705-RA" and "CG7705-RB." The first exon is at the left. The large deficiency *Df(3R)Exel6180* completely removes *vezl* together with 23 additional genes. Amino acid coding sequences (CDS) are in orange and untranslated regions (UTR) are in gray. (H) Sequence alignment of Vezatin family proteins. Black regions indicate conserved sequence and dark gray indicates >80% conserved sequence (ClustalW2). InterPro detects a "Vezatin domain" (purple bars) in vertebrate Vezatins and *Aspergillus* VezA but not in fly Vezl. Helical transmembrane domains predicted by two different algorithms are indicated by blue (InterPro) and red (SMART) bars. Green bars indicate low complexity regions predicted by PrDOS. A detailed amino acid alignment among fly Vezl, human Vezt, and the pfam12632 "Vezatin domain" consensus sequence is provided in Figure S1.
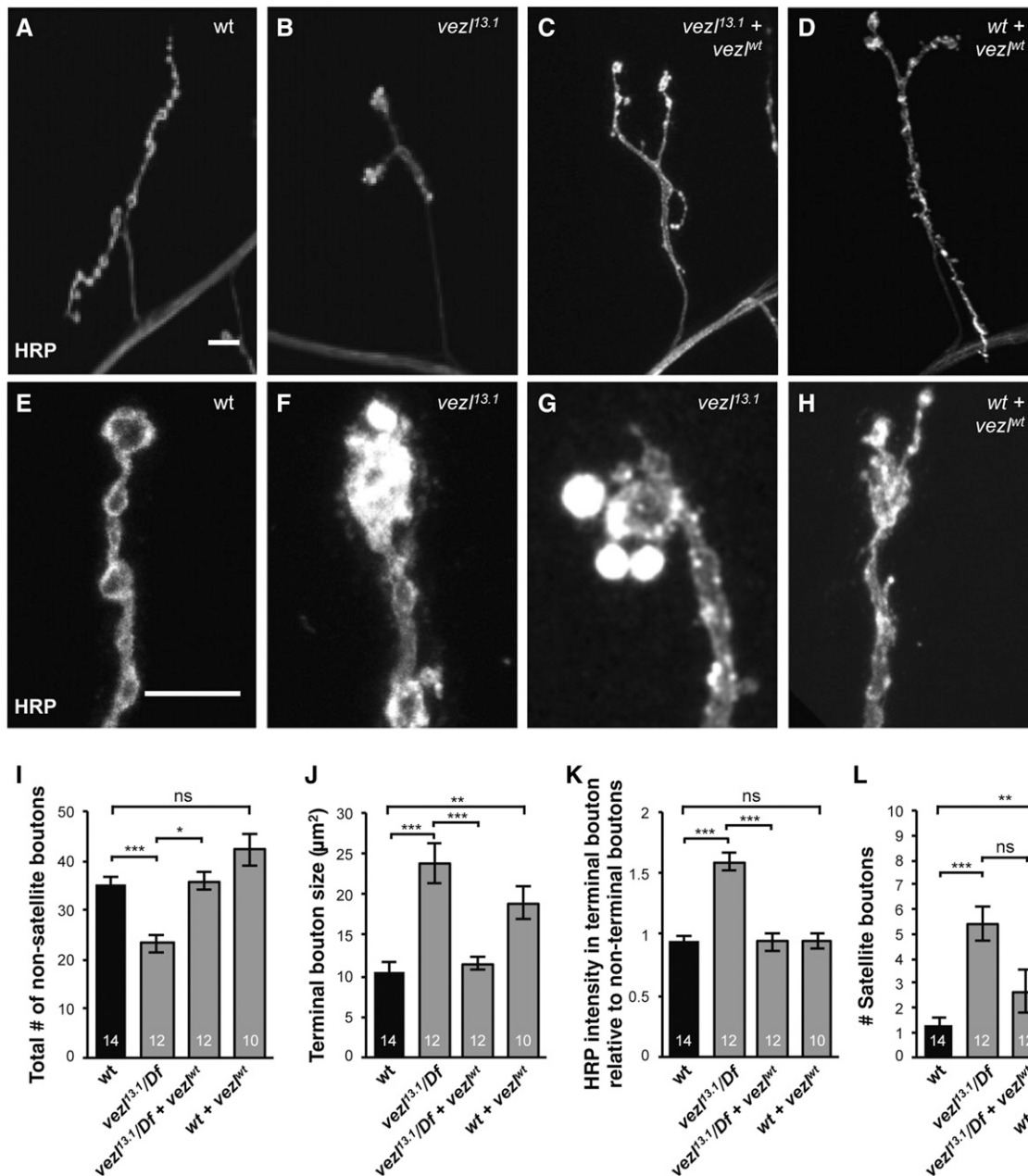
Figure 2 Vezl is required in larval motor neurons for normal NMJ size and terminal bouton morphology. (A–D) Third instar larval NMJs at muscle 4 in abdominal segment 3 (A3) stained with anti-HRP (white). Bar, 10 μm. (A) Wild type. (B) *vezl*[13.1]/*Df(3R)Exel6180* mutant NMJs have a reduced number of boutons. (C) Expression of a *vezl* cDNA in motor neurons of *vezl*[13.1]/*Df(3R)Exel6180* mutants restores NMJ size to that of wild type (quantified in I). (D) Expression of a *vezl* cDNA in motor neurons of wild-type animals increases the number of small, "satellite" boutons throughout the NMJ. (E–H) Larger magnifications of NMJs (different from those in A–D), stained with anti-HRP (white). Bar, 10 μm. (E) In wild type, the terminal bouton (top) and *en passant* boutons (below) have similar levels of anti-HRP staining. (F) In *vezl*[13.1]/*Df(3R)Exel6180* mutants, the terminal bouton (top) is often enlarged and contains significantly increased anti-HRP staining. Both defects are fully rescued by neuronal expression of a wild-type *vezl* transgene (quantified in J and K). (G) In *vezl*[13.1]/*Df(3R)Exel6180* mutants, the terminal bouton is often surrounded by satellite boutons containing increased anti-HRP staining. (H) Expression of a *vezl* cDNA in motor neurons of wild-type animals causes an increase in satellite boutons, including those that branch off the terminal bouton (as in this example). (I–L) Quantifications of the phenotypes mentioned in A–H. The number of animals is indicated on each bar. Error bars indicate SEM. *** $P < 0.001$, ** $P < 0.01$, * $P < 0.05$, based on two-tailed *t*-tests with Bonferroni correction. Means, SEMs, and *P*-values are available in Table S1.

have *721*-like short extensions that end in blobs (Figure 1, C and E). R7-specific expression of a *UAS-vezl* transgene constructed from the *vezl* cDNA with the largest open reading frame fully rescues the R7 defect (Figure 1, D and E). We conclude that *vezl* is required for normal R7 synaptic bouton morphology.

The observation that *vezl* loss causes late larval/early pupal lethality led us to wonder whether *vezl* might be generally
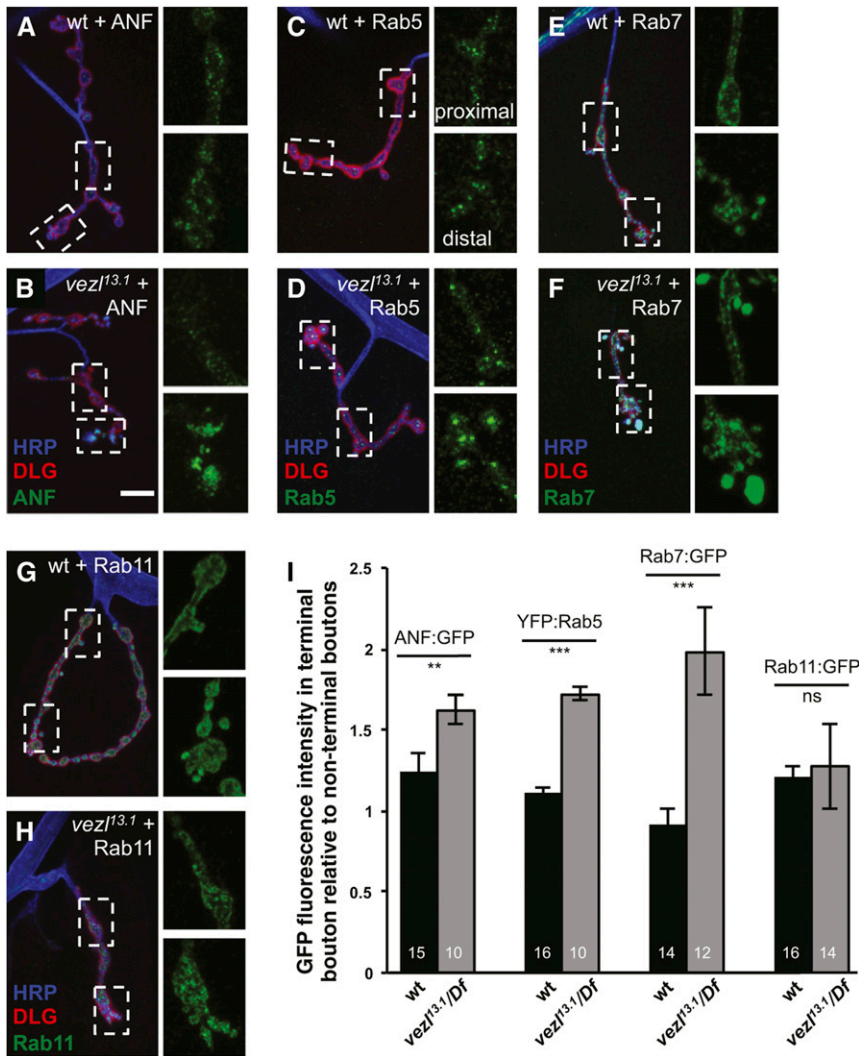
Figure 3 Loss of *vezl* causes an increase in DCVs and endosomes specifically in terminal boutons. (A–H) Third instar larval NMJs stained with anti-HRP (blue) and anti-Dlg (red). In each panel, dashed boxes indicate the regions containing *en passant* boutons (top) and terminal boutons (bottom) that are displayed with increased magnification in adjacent panels to the right. Bar, 10 μm. (A) In wild-type motor neurons, similar levels of the DCV marker ANF:GFP (green) localize to terminal and *en passant* boutons. (B) ANF:GFP is increased specifically in terminal boutons in *vezl¹³·¹/Df(3R)Exel6180* mutants. (C) In wild-type motor neurons, similar levels of the early endosome marker YFP:Rab5 (green) localize to terminal and *en passant* boutons. (D) YFP:Rab5 is increased specifically in terminal boutons in *vezl¹³·¹/Df(3R)Exel6180* mutants. (E) In wild-type motor neurons, similar levels of the early-late endosome marker Rab7:GFP (green) localize to terminal and *en passant* boutons. (F) Rab7:GFP is increased specifically in terminal boutons in *vezl¹³·¹/Df(3R)Exel6180* mutants. (G) In wild-type motor neurons, similar levels of the recycling endosome marker Rab11:GFP (green) localize to terminal and *en passant* boutons. (H) The localization of Rab11:GFP in *vezl¹³·¹/Df(3R)Exel6180* mutants resembles that in wild type. (I) Quantification of fluorescence intensities in A–H genotypes. The number of animals is indicated on each bar. Error bars indicate SEM. *** $P < 0.001$, ** $P < 0.01$, based on two-tailed *t*-tests. Means, SEMs, and *P*-values are available in Table S1.

required for synaptic bouton development. To test this, we turned to the larval NMJ. *vezl* loss was previously reported to disrupt mitotic spindles and chromosome segregation (Graziadio *et al.* 2018). However, we never observed missing NMJs or other gross abnormalities in axon morphology or targeting, indicating that *vezl* loss does not affect motor neuron survival or muscle target choice. We were therefore able to analyze Vezl's role in NMJ bouton development. We found that *vezl* mutants have significantly fewer boutons per NMJ than wild-type animals, a defect that is fully rescued by expression of a *UAS-vezl* transgene in motor neurons (Figure 2, A–C and I). In addition, Vezl loss specifically alters the morphology of NMJ terminal boutons, leaving all other (*i.e.*, *en passant*) boutons apparently unaffected. *vezl* mutant terminal boutons are abnormally large (Figure 2, E, F, and J) and stain more intensely with the neuronal membrane marker anti-HRP (Figure 2, E, F, and K). In addition, *vezl* mutant terminal boutons are frequently surrounded by smaller, "satellite" boutons that stain intensely with anti-HRP (Figure 2, G and L). We conclude that Vezl is required in both R7s and motor neurons for normal terminal bouton morphology. We note

that expressing Vezl in wild-type motor neurons has gain-of-function effects that are superficially similar to defects caused by Vezl loss: an increase in terminal bouton size and an increase in satellite bouton number (Figure 2, H, J, and L). However, the Vezl gain and loss effects are likely distinct: Vezl gain induces satellite boutons along the whole length of the NMJ instead of specifically from the terminal bouton, and does not cause an accumulation of HRP in the terminal bouton. Finally, we note that expressing Vezl specifically in motor neurons does not rescue the lethality caused by Vezl loss, consistent with its previously described broader effects on development (Graziadio *et al.* 2018).

Vezl loss results in excessive DCVs and endosomes in terminal boutons and disrupts retrograde BMP signaling

Many different manipulations can cause a decrease in bouton number or increase in satellite boutons in fly larval NMJs. However, the only previously reported instance of enlarged terminal boutons with increased anti-HRP staining is that caused by disrupting essential components of the dynein-dynactin complex in motor neurons: knockdown of dynactin
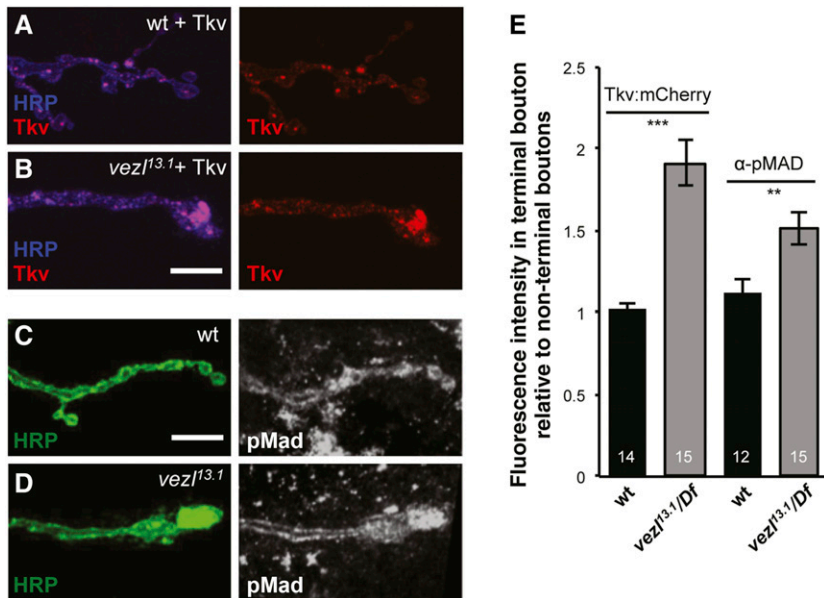
Figure 4 Loss of *vezl* disrupts retrograde BMP signaling. (A and B) Third instar larval NMJs stained with anti-HRP (blue) in which motor neurons express Tkv:mCherry (red). Each terminal bouton is on the right. Bar, 10 μm. (A) In wild-type motor neurons, similar levels of the BMP type I receptor marker Tkv:mCherry (red) localize to terminal and *en passant* boutons. (B) Tkv:mCherry is increased specifically in terminal boutons in *vezl[13.1]/Df(3R)Exel6180* mutants. (C and D) Third instar larval NMJs stained with anti-HRP (green) and anti-pMad (white). (C) In wild type, similar levels of phosphorylated Mad (pMad), the downstream target of BMP signaling in motor neurons, localize to terminal and *en passant* boutons. (D) Anti-pMad staining is increased specifically in terminal boutons in *vezl[13.1]/Df(3R)Exel6180* mutants. (E) Quantification of staining intensities in A–D genotypes. The number of animals is indicated on each bar. Error bars indicate SEM. *** $P <$ 0.001, ** $P <$ 0.01, based on two-tailed *t*-tests. Means, SEMs, and *P*-values are available in Table S1.

or dynein subunits traps dynein-dependent cargoes such as DCVs and endosomes in terminal boutons, causing the latter to expand in size (Lloyd *et al.* 2012). To test whether Vezl might also be involved in this process, we first examined the localization of retrograde cargoes in fixed samples. When expressed in fly neurons, ANF:GFP, a fusion of GFP to a rat neuropeptide, is packaged and transported in DCVs in the same way as endogenous neuropeptides (Rao *et al.* 2001; Levitan *et al.* 2007; Wong *et al.* 2012). We found that Vezl loss, like loss of the essential dynactin subunit p150[Glued], increases ANF:GFP specifically in terminal boutons (Figure 3, A, B, and I; Lloyd *et al.* 2012). The early endosome marker YFP:Rab5 and the late endosome marker Rab7:GFP also accumulate in terminal boutons in the absence of p150[Glued] (Lloyd *et al.* 2012). We found that both of these endosome markers are likewise specifically increased in terminal boutons in *vezl* mutants (Figure 3, C–F, and I). By contrast, the recycling endosome marker Rab11:GFP, which does not normally undergo retrograde transport, and the synaptic vesicle protein CSP do not show such an increase in *vezl* mutants (Figure 3, G–I and Figure S2, A and B). Similarly, the major active zone protein Brp is not increased: instead, the density of Brp puncta in terminal boutons is decreased by *vezl* loss, although these puncta remain apposed to postsynaptic glutamate receptors, as in wild type (Figure S2, C and E).

The increase in ANF:GFP, YFP:Rab5, and Rab7:GFP in NMJ terminal boutons implicate Vezl in the initiation of their retrograde transport and suggest a potential explanation for the reduced NMJ size in *vezl* mutants. Normal NMJ growth requires motor neurons to transduce a muscle-released BMP signal through the axon to the nucleus [McCabe *et al.* 2003; reviewed in Deshpande and Rodal (2016)]. The BMP signal binds the receptors Wishful thinking (Wit), Saxophone (Sax), and Thick veins (Tkv), which phosphorylate the transcription factor Mothers Against Dpp

(Mad). Phosphorylated Mad (pMad) can then enter the motor neuron nucleus and activate transcription of growth-promoting factors (Aberle *et al.* 2002; Marqués *et al.* 2002; McCabe *et al.* 2003; Rawson *et al.* 2003; McCabe *et al.* 2004). Previous work has shown that pMad is not retrogradely transported (Smith *et al.* 2012). Instead, entry of pMad into the nucleus depends on the retrograde transport of activated BMP receptors that have been endocytosed (Smith *et al.* 2012). To determine Vezl's effect on this pathway, we examined the localization of a tagged form of the BMP receptor Tkv. In fixed samples, Tkv:mCherry normally localizes to puncta distributed throughout the motor neuron axon and boutons (Figure 4A). We found that Vezl loss causes an increase in Tkv:mCherry specifically in terminal boutons (Figure 4, D and E), consistent with a defect in its retrograde transport. Previous work has shown that BMP signaling also acts locally, phosphorylating Mad within synaptic boutons by a pathway that does not require retrograde transport (O'Connor-Giles *et al.* 2008; Higashi-Kovtun *et al.* 2010; Sulkowski *et al.* 2016). This presynaptic pMad participates with postsynaptic glutamate receptors in a positive feedback loop that regulates the distribution of glutamate receptor subtypes (Sulkowski *et al.* 2016). We were unable to detect nuclear pMad staining above background in either wild type or *vezl* mutants. However, we did find that pMad levels are significantly increased in *vezl* mutant terminal boutons (Figure 4, C–E), suggesting that Vezl loss traps activated Tkv in terminal boutons, preventing the increase in NMJ bouton number that depends on retrograde BMP signaling.

Vezl is required for the retrograde movement of Tkv out of terminal boutons

We next directly tested the effect of Vezl loss on the movement of individual vesicles in live animals. We first tracked the movement of Tkv:mCherry. In wild-type animals, significantly
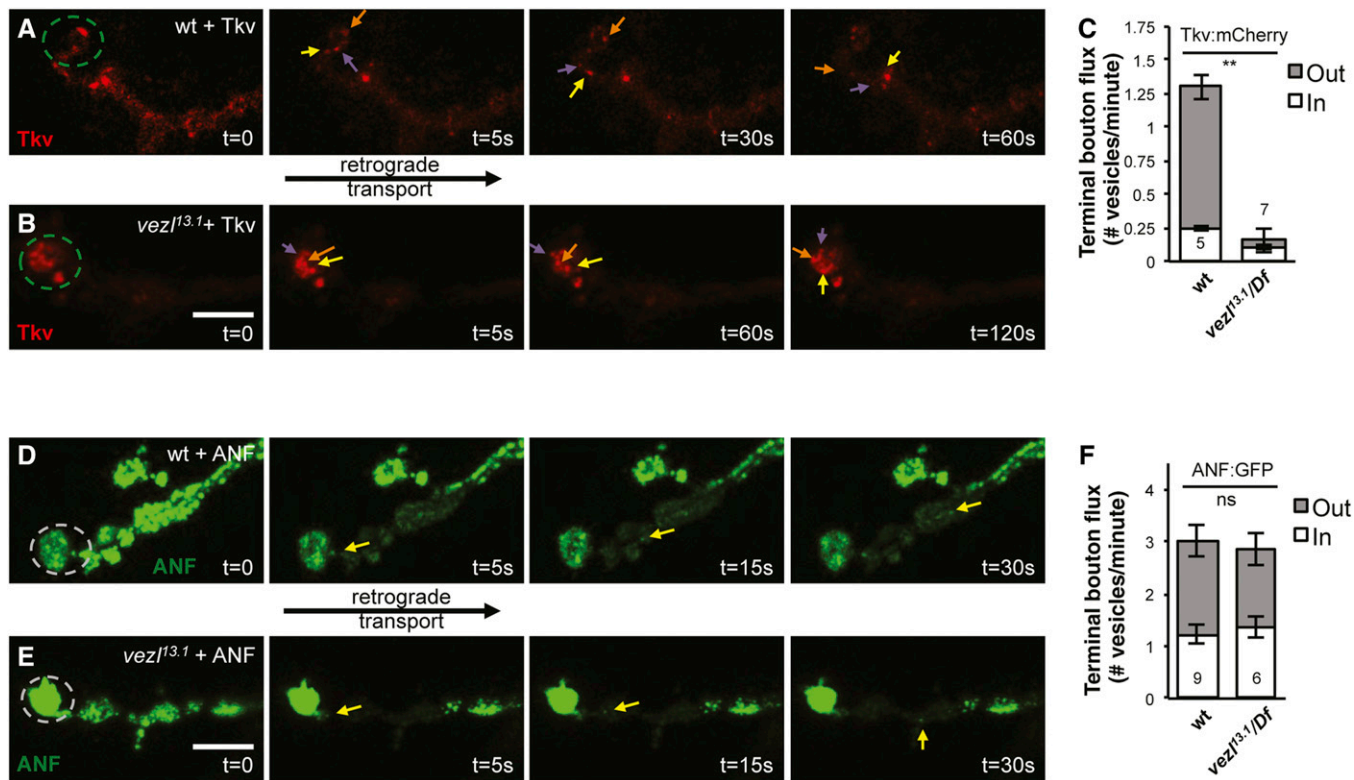
Figure 5 Vezl is required for the retrograde movement of Tkv out of terminal boutons. (A, B, D, and E) Time courses of vesicle movements in live third instar larvae. Each terminal bouton is on the left (dashed circles) and retrograde transport occurs toward the right. Bar, 10 μm. (A) In wild type, Tkv:mCherry puncta (red; arrows) frequently move retrogradely out of the terminal bouton. (B) Tkv:mCherry puncta (red; arrows) in *vezl*[13.1]/*Df(3R) Exel6180* mutants often fail to exit the terminal bouton and instead circulate in an unorganized fashion. Note the extended recording time compared to that in A. Note that B is shown with reduced brightness relative to A, so that individual puncta are more evident. (C) Quantification of Tkv:mCherry movement. Retrograde movement out of the terminal bouton is significantly decreased in *vezl* mutants. The number of animals is indicated on each bar. Error bars indicate SEM. ** $P < 0.01$, based on two-tailed *t*-tests. Means, SEMs, and *P*-values are available in Table S1. (D and E) Regions adjacent to the terminal bouton were photobleached, allowing the movements of individual ANF:GFP puncta into the bleached region to be monitored. (D) In wild type, ANF:GFP puncta (green; arrows) frequently move retrogradely out of the terminal bouton. Note that the angle of the single *z*-section in this example creates an illusion that, before photobleaching, ANF:GFP is higher in the nonterminal boutons than in the terminal bouton; there is no such difference (see Figure 3, A and I). (E) The movement of ANF:GFP puncta (green; arrows) in *vezl*[13.1]/*Df(3R)Exel6180* mutants is similar to that in wild type. (F) Quantification of ANF:GFP movement. The number of animals is indicated on each bar. Error bars indicate SEM. *P*-value was not significant based on two-tailed *t*-tests. Means, SEMs, and *P*-values are available in Table S1.

more Tkv:mCherry puncta move out of the terminal bouton, *i.e.*, retrogradely, than in the opposite direction (Figure 5, A and C). By contrast, in *vezl* mutant animals, very few Tkv:mCherry puncta move out of terminal boutons (Figure 5, B and C). Instead, most Tkv:mCherry puncta within *vezl* mutant terminal boutons move sporadically and nondirectionally (Figure 5B), suggesting that they are not moving along microtubule tracks. We conclude that *vezl* is required for the initiation of Tkv:mCherry retrograde transport out of terminal boutons.

The possibility remained that *vezl* loss might only affect Tkv:mCherry transport indirectly, perhaps by causing the accumulation of excess HRP-positive membrane. If so, one would expect that most or all retrogradely transported cargoes would be similarly affected. Therefore, we next tracked the movement of individual ANF:GFP puncta. Because these puncta are more numerous than Tkv:mCherry puncta and therefore difficult to follow individually, we used FRAP. We

photobleached the boutons adjacent to the terminal bouton and measured the number of vesicles that entered the bleached area either by retrograde transport from the terminal bouton or by anterograde transport from more proximal boutons. As expected of cargoes that use retrograde transport to circulate among *en passant* boutons, we found that ANF:GFP puncta do not display the bias toward retrograde movement that we observed for Tkv:mCherry puncta: in wild-type animals, roughly equal numbers of ANF:GFP puncta move out of and toward the terminal bouton (Figure 5, D and F). We found that *vezl* loss does not significantly alter anterograde or retrograde flux of ANF:GFP at terminal boutons (Figure 5, E and F). The mild increase in ANF:GFP levels in terminal boutons (Figure 3, B and I) suggests that a subtle defect may nonetheless exist and manifest as a slow accumulation over time. However, our live imaging indicates that, despite its strong effect on Tkv:mCherry, Vezl loss does not uniformly prevent retrograde cargoes from exiting the terminal boutons.
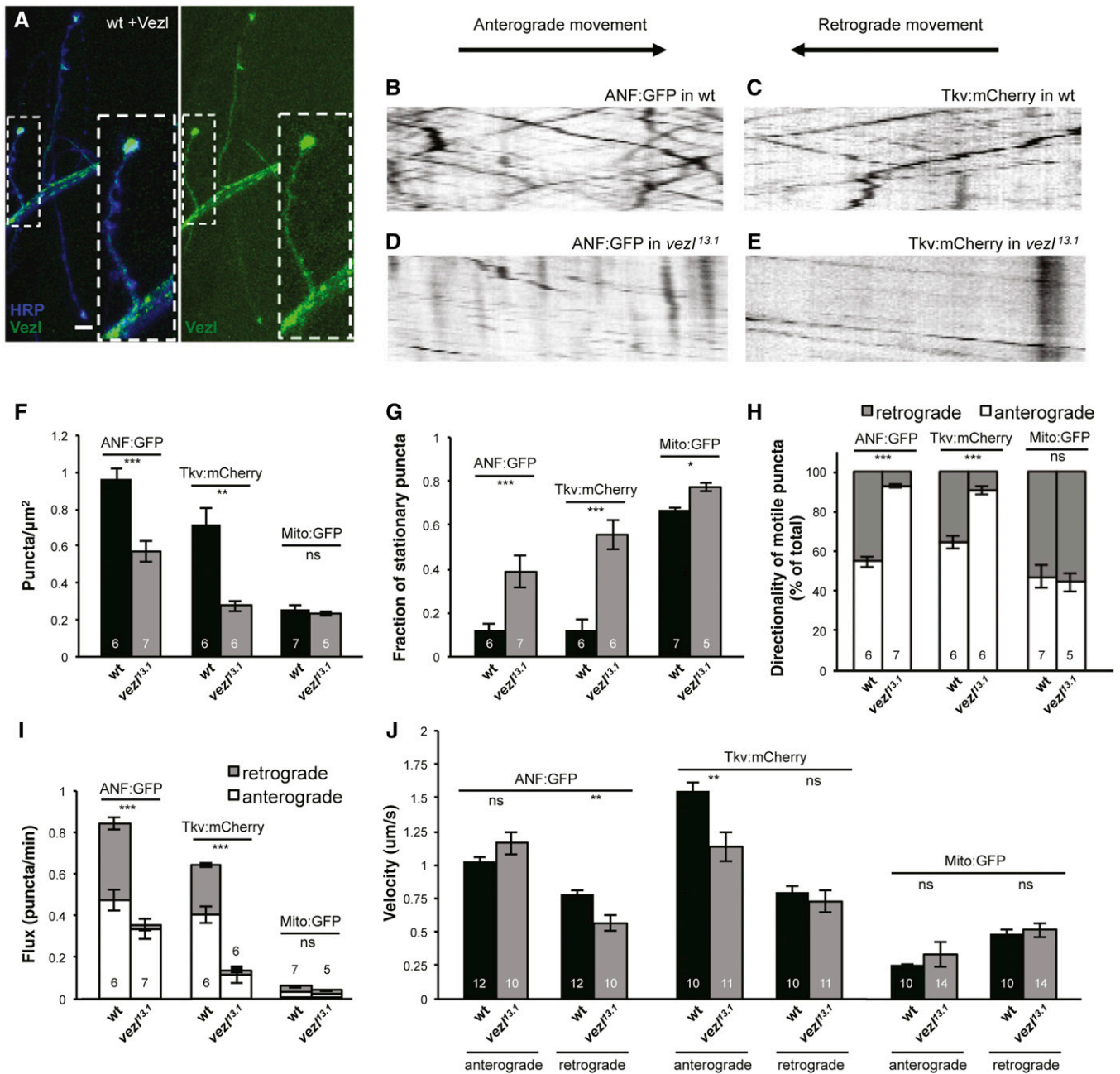
Figure 6 Vezl is enriched in terminal boutons but is also required for normal transport of DCVs and Tkv along axons. (A) NMJ from a wild-type third instar larva containing two copies each of the motor neuron driver *OK371-Gal4* and the *UAS-Vezl^wt:Venus* transgene. Larvae were dissected, but not fixed, and fluorescence-conjugated anti-HRP (blue) was added to the dissection media. Vezl:Venus (green) is highest in terminal boutons but also present in *en passant* boutons and the axon shaft. (Vezl:Venus was difficult to detect in fixed samples or in animals containing fewer transgenes.) Bar, 10 μm. Most Vezl:Venus signal appears to be stationary, but we did observe movement of some Vezl:Venus puncta within axon bundles (Movie S1). (B–E) Representative kymographs of (B and D) ANF:GFP or (C and E) Tkv:mCherry in third instar larval axons; for experiments in B–J, one bundle of axons was imaged per animal, near the ventral nerve cord. The *x*-axes represent distance and the *y*-axes represent time. Lines that slope downward from left to right are puncta moving in the anterograde direction; lines that slope downward from right to left are puncta moving in the retrograde direction. Stationary puncta result in vertical lines. In wild type, (B) ANF:GFP and (C) Tkv:mCherry puncta move in both directions. In *vezl^13.1/Df(3R)Exel6180* mutants, retrograde movement of (D) ANF:GFP and (E) Tkv:mCherry puncta is considerably reduced. (F–J) Quantification of ANF:GFP, Tkv:mCherry, and Mito:GFP movement in wild type and *vezl^13.1/Df(3R)Exel6180* mutants. Loss of *vezl* decreases the density of ANF:GFP and Tkv:mCherry puncta within axons (F), increases the fraction of those puncta that are stationary (G), and decreases the proportion of motile ANF:GFP and Tkv:mCherry puncta that are moving in the retrograde direction (H), resulting in a severe decrease in their retrograde flux (I). *vezl* loss also affects the velocities of ANF:GFP and Tkv:mCherry puncta (J). By contrast, we observed only a mild effect of *vezl* loss on Mito:GFP movement (F–J). In all bar graphs, the number of animals is indicated on each bar. Error bars indicate SEM. * $P < 0.05$, ** $P < 0.01$, *** $P < 0.001$, based on two-tailed *t*-tests. Means, SEMs, and *P*-values are available in Table S1.
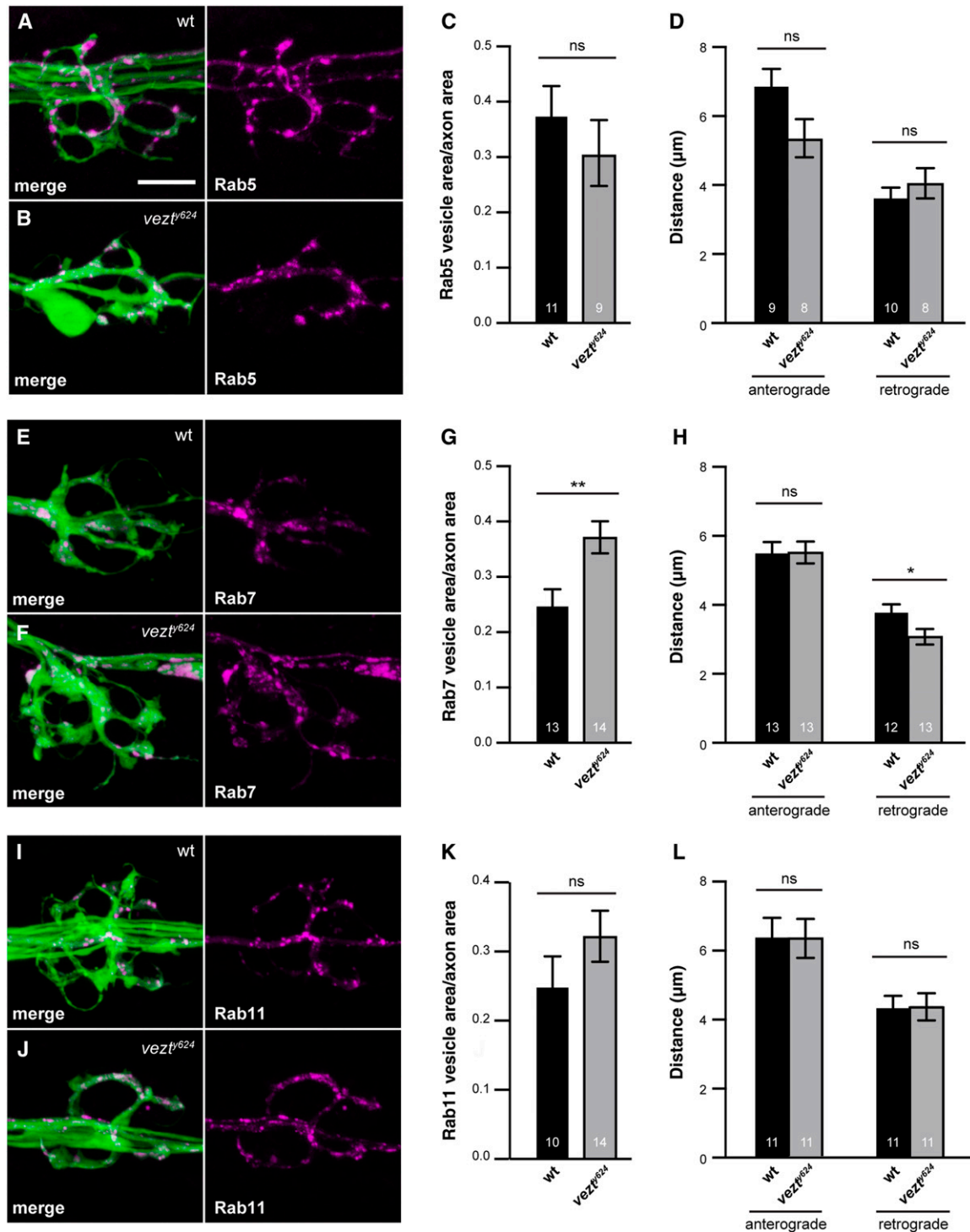
Figure 7 Zebrafish *vezt* mutants have decreased retrograde transport of late endosomes, which accumulate in axon terminals. (A, B, E, F, I, and J) pLL axon terminals marked by cytoplasmic GFP (green) in the *TgBAC(neurod:egfp)*[nl1] transgenic line. Axon terminal swellings caused by *vezt* loss are particularly evident in B (see also Figure S4 and the quantification of wild-type and *vezt* mutant axon terminal volumes in *Results*). Animals were mosaic for transgenes driving neuronal expression of (A–D) Rab5:mRFP, (E–H) Rab7:mRFP, or (I–L) Rab11:RFP. Because of this mosaicism and the axon terminal swelling caused by *vezt* loss, Rab accumulation was assessed in C, G, and K by normalizing Rab area to axon terminal area. Normalizing instead to axon terminal number yielded similar results (see Table S1). Bar, 10 μm. (A and B) The accumulation of Rab5:mRFP (magenta) in axon terminals is similar in (A) wild-type and (B) *vezt*[y624] mutant animals. Quantified in C and D, which also shows largely normal movement of Rab5:mRFP. (E and F) By contrast, Rab7:mRFP (magenta) accumulates significantly more in (F) *vezt*[y624] mutant axon terminals than in (E) wild-type terminals. Quantified in G and H, which also shows a decreased retrograde transport distance in *vezt*[y624] mutants. (I–L) Rab11:mRFP accumulation and movement are unaffected by *vezt* loss. In all bar graphs, the number of animals is indicated on each bar. Error bars indicate SEM. * $P < 0.05$, ** $P < 0.01$, based on two-way ANOVA. Means, SEMs, and *P*-values are available in Table S1.

Vezl is enriched in terminal boutons but is also required for normal transport of DCVs and Tkv along axons

Retrograde transport out of terminal boutons is initiated when dynein-cargo complexes are loaded onto microtubules by the dynactin subunit p150^{Glued} (Lloyd *et al.* 2012; Moughamian and Holzbaur 2012; Moughamian *et al.* 2013). Presumably to facilitate this, p150^{Glued} is highly enriched in terminal boutons, unlike dynein itself (Lloyd *et al.* 2012; Moughamian and Holzbaur 2012). To test whether Vezl might specifically regulate transport out of terminal boutons, we examined Vezl localization by driving expression of Venus-tagged full-length Vezl in motor neurons of wild-type animals. Detecting Vezl:Venus signal requires two copies each of *OK371-Gal4* and *UAS-Vezl:Venus*, resulting, presumably, in considerable overexpression. Under these conditions, Vezl:Venus is highly enriched in terminal boutons, consistent with its role in transport initiation (Figure 6A). However, Vezl:Venus is also present at lower levels in nonterminal boutons and along axon shafts. While most Vezl:Venus signal appears to be stationary, we did observe occasional movement of Vezl:Venus puncta in both anterograde and retrograde directions (Movie S1).

To test whether Vezl might be required for normal transport within axons, we tracked the movement of ANF:GFP, Tkv:mCherry, and the mitochondrial marker Mito:GFP in nerve bundles emerging from the ventral nerve cord. We found that Vezl loss decreases the density of ANF:GFP and Tkv:mCherry puncta within axons and increases the proportion of these puncta that are stationary (Figure 6, B–G). As a consequence, both anterograde and retrograde flux of Tkv:mCherry is decreased, as is retrograde flux of ANF:GFP (Figure 6I). The effect on retrograde flux is particularly striking: Vezl loss significantly decreases the proportion of motile ANF:GFP and Tkv:mCherry puncta that move in the retrograde direction (Figure 6H). By contrast, Vezl loss does not alter the number of Mito:GFP puncta present within axons (Figure 6F) and does not have a specific effect on retrograde Mito:GFP transport, although there is a slight increase in the proportion of Mito:GFP that are stationary (Figure 6G). Together, these results indicate that Vezl is strongly required for the retrograde transport of DCVs and signaling endosomes in axons, but is largely dispensable for mitochondrial transport. We note that Vezl loss decreases the velocities of retrograde ANF:GFP and anterograde Tkv:mCherry movement (Figure 6J), but how this might relate to the other axon transport defects is unclear.

Loss of vezt in zebrafish impairs retrograde transport of Rab7-positive endosomes

Vertebrate Vezt has not previously been implicated in axonal transport. To test its potential role in this process, we first examined whether expression of tagged hVezt might rescue fly *vezl* mutant NMJ defects, despite the low amino acid sequence identity between the fly and human proteins. We found that, unlike fly Vezl, hVezt expressed in fly motor neurons is not enriched at terminal boutons and does not restore either NMJ size or terminal bouton morphology in *vezl*

mutants (Figure S3). We therefore turned to a vertebrate model system, zebrafish, to directly test whether vertebrate Vezt plays a role in retrograde axonal transport. The pLL sensory axons of the larval zebrafish are ideal for analyses of cargo localization and transport in axons, in part because of their considerable length (Drerup and Nechiporuk 2016). We used CRISPR technology to create a zebrafish line, *vezt^{y624}*, in which the single *vezt* ortholog within the zebrafish genome is disrupted. In this line, a 5-bp insertion in exon three disrupts the open reading frame, leading to a 40 amino acid insertion and premature stop site. We found that *vezt^{y624}* homozygotes are grossly normal but die by late larval stages.

As in fly, loss of dynein or dynactin in zebrafish causes retrogradely transported cargoes to accumulate in axon terminals, resulting in characteristic axon terminal swellings (Drerup and Nechiporuk 2013; Drerup *et al.* 2017). We found that at 4 dpf, pLL axon terminals in *vezt* mutant zebrafish are noticeably swollen: quantification of axon terminal volume revealed a significant increase in *vezt* mutants compared to their wild-type siblings (638 ± 49 μm^3 *vs.* 417 ± 63 μm^3; Figure S4, A–F). To determine whether loss of retrograde cargo movement correlated with this defect, we first analyzed the localization of dynein and dynactin components in pLL axons by immunofluorescence. We found that excess p150 accumulates in *vezt* mutant terminals as compared to wild-type siblings at 4 dpf (Figure S4, A, B, and G), suggestive of a defect in retrograde transport. Dynein heavy chain and mitochondria are localized normally (Figure S4, C–G).

To directly assess the localization and transport of endosome subtypes, we mosaically expressed mRFP-tagged Rab5, Rab7, and Rab11 in pLL neurons of live larvae. We found that mRFP:Rab7-positive late endosomes significantly accumulate in pLL axon terminals in *vezt* mutants at 4 dpf, while Rab5- and Rab11-labeled endosomes localize normally (Figure 7, A–C, E–G, and I–K). We then analyzed the movement of these markers in axons and found that retrograde transport of mRFP:Rab7-positive endosomes is specifically impaired in *vezt* mutants, as assessed by distance traveled (Figure 7H); Rab5-positive early endosome anterograde transport showed a modest decrease that failed to reach significance (Figure 7D), and recycling endosomes moved normally (Figure 7L). We conclude that Vezt is required for normal retrograde transport of Rab7-labeled endosomes in vertebrate axons.

Discussion

Here, we describe the identification of a Vezt-like fly protein, Vezl, that is enriched at NMJ terminal boutons and required for normal retrograde transport of a subset of cargos. In the absence of Vezl, Rab5- and Rab7-positive endosomes, including signaling endosomes, and DCVs accumulate within NMJ terminal boutons. The retrograde movement of signaling endosomes and DCVs, but not of mitochondria, is also impaired within axon shafts. We find that loss of Vezt from zebrafish impairs the retrograde movement of Rab7-labeled endosomes in sensory axons. This work identifies a new, conserved regulator of dynein-dependent endosomal transport in neurons.

While neither fly Vezl nor vertebrate Vezt have previously been implicated in axonal transport, a distantly related *Aspergillus* protein, VezA, is required for the dynein-dependent retrograde transport of endosomes in hyphae (Yao *et al.* 2015). Tagged VezA is enriched at microtubule plus ends within hyphal tips as Vezl is at terminal boutons, and loss of VezA decreases the frequency of retrograde endosome movement, causing endosomes to accumulate at microtubule plus ends (Yao *et al.* 2015). VezA is thought to act by promoting binding between the endosome-specific cargo adaptor HookA and the dynein-dynactin complex (Yao *et al.* 2015). Might Vezl and Vezt act similarly?

While the Hook family of cargo adaptors is conserved across species (Xiang *et al.* 2015; Reck-Peterson *et al.* 2018), the single Hook protein in fly does not seem to be required for retrograde axonal transport of endosomes. Fly Hook can associate with Rab5- and Rab7-positive endosomes and has some effects on endosome trafficking (Krämer and Phistry 1999). However, hook null mutants are viable (Krämer and Phistry 1999; Sunio *et al.* 1999; Szatmári *et al.* 2014), their NMJs do not have the terminal bouton swelling that is characteristic of *vezl* mutants (Narayanan *et al.* 2000), and their NMJs have more boutons rather than fewer (Narayanan *et al.* 2000). The cargo specificity of Vezl toward endosomes and, to a lesser extent, DCVs, but not mitochondria, indicates that, like VezA, Vezl does not alter the general properties of the dynein-dynactin motor or its microtubule substrate. Instead, Vezl likely promotes interactions between cargoes and dynein-dynactin that are required for the initiation of retrograde transport both out of terminal boutons and within axon shafts. Such interactions could be direct or could instead involve another cargo adaptor such as Bicaudal, which shares a similar structure and interaction space on the dynein motor with Hook proteins (McKenney *et al.* 2014; Schlager *et al.* 2014; Urnavicius *et al.* 2018).

Unlike fly Hook, vertebrate Hooks are well established as activating adaptors for cargo-bound dynein-dynactin (Reck-Peterson *et al.* 2018). Zebrafish Vezt may therefore act analogously to VezA and promote binding between the Rab7-specific Hook protein Hook3 and Rab7 endosome-bound dynein-dynactin. Vertebrate Vezt was originally identified based on its association with cell-cell junction proteins, including the cadherin-catenin complex within epithelial cells (Küssel-Andermann *et al.* 2000; Hyenne *et al.* 2005), PSD95 within hippocampal dendrites (Danglot *et al.* 2012), and, more recently, muscle acetylcholine receptor at NMJs (Koppel *et al.* 2019). Consistent with this localization pattern, Vezt is required for the maturation and maintenance of adherens junctions (Hyenne *et al.* 2005; Hyenne *et al.* 2007), dendrites (Sanda *et al.* 2010; Danglot *et al.* 2012), and NMJ synapses (Koppel *et al.* 2019). The precise mechanism by which Vezt has these effects is unclear, but its binding partners include the small GTPase Arf6 (Sanda *et al.* 2010), which regulates dynein-dependent endosome movements during cytokinesis, exocytosis, and macropinocytosis (Montagnac *et al.* 2009; Marchesin *et al.* 2015; Williamson and Donaldson 2019). It is therefore possible that Vezt's ability to interact with Arf6 contributes to its regulation of endosome movement in axons.

A significant consequence of Vezl loss at fly NMJ is its disruption of neurotrophic BMP signaling. The failure of Tkv to undergo retrograde transport out of terminal boutons provides a simple explanation for the reduced number of boutons at *vezl* mutant NMJs. The observation that pMad is increased in *vezl* mutant terminal boutons suggests that Vezl loss does not prevent the trafficking of activated receptors into endosomes, but instead specifically prevents their retrograde transport. Like p150[Glued], Vezl is normally enriched in NMJ terminal boutons, suggesting that, like p150[Glued], Vezl is particularly important in initiating this process.

vezl loss was previously found to disrupt the behavior of mitotic and meiotic spindles and their attachment to chromosomes (Graziadio *et al.* 2018). Despite this defect, we did not observe missing NMJs, and *vezl* mutants do not die until they are late larvae or early pupae; this may be because wild-type *vezl* mRNA is present in the maternal germline (Fisher *et al.* 2012). Graziadio *et al.* (2018) did not recognize the similarity of Vezl to vertebrate Vezt or identify the mechanism by which Vezl affects spindle behavior. One possibility is that Vezl regulates dynein-dynactin-dependent movements during cell division as well as in axons. In support of this, Graziadio *et al.* (2018) observed that Vezl loss causes the failure of a dynein-dependent event during mitosis: in *vezl* mutants, the dynein-associated protein Zw10 fails to spread along spindle microtubules and instead accumulates at kinetochores. Alternatively, like vertebrate Vezt, Vezl may have functions that are independent of its effects on dynein-dependent transport.

Acknowledgments

Literature Cited

Aberle, H., A. P. Haghighi, R. D. Fetter, B. D. McCabe, T. R. Magalhães *et al.*, 2002 *Wishful thinking* encodes a BMP type II receptor that regulates synaptic growth in *Drosophila*. Neuron 33: 545–558. https://doi.org/10.1016/S0896-6273(02)00589-5

Ashburner, M., 1989 *Drosophila: A Laboratory Manual*. Cold Spring Harbor Laboratory Press, Cold Spring Harbor.

Bahloul, A., M. C. Simmler, V. Michel, M. Leibovici, I. Perfettini *et al.*, 2009 Vezatin, an integral membrane protein of adherens junctions, is required for the sound resilience of cochlear hair cells. EMBO Mol. Med. 1: 125–138. https://doi.org/10.1002/emmm.200900015

Ball, R. W., M. Warren-Paquin, K. Tsurudome, E. H. Liao, F. Elazzouzi *et al.*, 2010 Retrograde BMP signaling controls synaptic growth at the NMJ by regulating Trio expression in motor neurons. Neuron 66: 536–549. https://doi.org/10.1016/j.neuron.2010.04.011

Burger, A., H. Lindsay, A. Felker, C. Hess, C. Anders *et al.*, 2016 Maximizing mutagenesis with solubilized CRISPR-Cas9 ribonucleoprotein complexes. Development 143: 2025–2037. https://doi.org/10.1242/dev.134809

Carrington, B., G. K. Varshney, S. M. Burgess, and R. Sood, 2015 CRISPR-STAT: an easy and reliable PCR-based method to evaluate target-specific sgRNA activity. Nucleic Acids Res. 43: e157. https://doi.org/10.1093/nar/gkv802

Danglot, L., T. Freret, N. Le Roux, N. Narboux Nême, A. Burgo *et al.*, 2012 Vezatin is essential for dendritic spine morphogenesis and functional synaptic maturation. J. Neurosci. 32: 9007–9022. https://doi.org/10.1523/JNEUROSCI.3084-11.2012

Deshpande, M., and A. A. Rodal, 2016 The crossroads of synaptic growth signaling, membrane traffic and neurological disease: insights from *Drosophila*. Traffic 17: 87–101. https://doi.org/10.1111/tra.12345

Drerup, C. M., and A. V. Nechiporuk, 2013 JNK-interacting protein 3 mediates the retrograde transport of activated c-Jun N-terminal kinase and lysosomes. PLoS Genet. 9: e1003303. https://doi.org/10.1371/journal.pgen.1003303

Drerup, C. M., and A. V. Nechiporuk, 2016 *In vivo* analysis of axonal transport in zebrafish. Methods Cell Biol. 131: 311–329. https://doi.org/10.1016/bs.mcb.2015.06.007

Drerup, C. M., A. L. Herbert, K. R. Monk, and A. V. Nechiporuk, 2017 Regulation of mitochondria-dynactin interaction and mitochondrial retrograde transport in axons. eLife 6: e22234. https://doi.org/10.7554/eLife.22234

Fisher, B., R. Weiszmann, E. Frise, A. Hammonds, P. Tomancak *et al.*, 2012 BDGP In Situ Homepage. Available at: http://insitu.fruitfly.org/cgi-bin/ex/insitu.pl. Accessed: April 14, 2020.

Graziadio, L., V. Palumbo, F. Cipressa, B. C. Williams, G. Cenci *et al.*, 2018 Phenotypic characterization of *diamond* (*dind*), a *Drosophila* gene required for multiple aspects of cell division. Chromosoma 127: 489–504. https://doi.org/10.1007/s00412-018-0680-y

Guedes-Dias P., and E. L. F. Holzbaur, 2019 Axonal transport: Driving synaptic function. Science 366: eaaw9997. https://doi.org/10.1126/science.aaw9997

Guo, W., K. Stoklund Dittlau, and L. Van Den Bosch, 2020 Axonal transport defects and neurodegeneration: molecular mechanisms and therapeutic implications. Semin. Cell Dev. Biol. 99: 133–150. https://doi.org/10.1016/j.semcdb.2019.07.010

Higashi-Kovtun, M. E., T. J. Mosca, D. K. Dickman, I. A. Meinertzhagen, and T. L. Schwarz, 2010 Importin-beta11 regulates synaptic phosphorylated mothers against decapentaplegic, and thereby influences synaptic development and function at the *Drosophila* neuromuscular junction. J. Neurosci. 30: 5253–5268. https://doi.org/10.1523/JNEUROSCI.3739-09.2010

Hyenne, V., S. Louvet-Vallée, A. El-Amraoui, C. Petit, B. Maro *et al.*, 2005 Vezatin, a protein associated to adherens junctions, is required for mouse blastocyst morphogenesis. Dev. Biol. 287: 180–191. https://doi.org/10.1016/j.ydbio.2005.09.004

Hyenne, V., C. Souilhol, M. Cohen-Tannoudji, S. Cereghini, C. Petit *et al.*, 2007 Conditional knock-out reveals that zygotic *vezatin*-null mouse embryos die at implantation. Mech. Dev. 124: 449–462. https://doi.org/10.1016/j.mod.2007.03.004

Kimmel, C. B., W. W. Ballard, S. R. Kimmel, B. Ullmann, and T. F. Schilling, 1995 Stages of embryonic development of the zebrafish. Dev. Dyn. 203: 253–310. https://doi.org/10.1002/aja.1002030302

Koppel, N., M. B. Friese, H. L. Cardasis, T. A. Neubert, and S. J. Burden, 2019 Vezatin is required for the maturation of the neuromuscular synapse. Mol. Biol. Cell 30: 2571–2583. https://doi.org/10.1091/mbc.E19-06-0313

Krämer, H., and M. Phistry, 1999 Genetic analysis of *hook*, a gene required for endocytic trafficking in *Drosophila*. Genetics 151: 675–684. https://www.genetics.org/content/151/2/675

Küssel-Andermann, P., A. El-Amraoui, S. Safieddine, S. Nouaille, I. Perfettini *et al.*, 2000 Vezatin, a novel transmembrane protein, bridges myosin VIIA to the cadherin-catenins complex. EMBO J. 19: 6020–6029. https://doi.org/10.1093/emboj/19.22.6020

Lee, T., and L. Luo, 1999 Mosaic analysis with a repressible cell marker for studies of gene function in neuronal morphogenesis. Neuron 22: 451–461. https://doi.org/10.1016/S0896-6273(00)80701-1

Lee, C. H., T. G. Herman, T. R. Clandinin, R. Lee, and S. L. Zipursky, 2001 N-cadherin regulates target specificity in the *Drosophila* visual system. Neuron 30: 437–450. https://doi.org/10.1016/S0896-6273(01)00291-4

Levitan, E. S., F. Lanni, and D. Shakiryanova, 2007 *In vivo* imaging of vesicle motion and release at the *Drosophila* neuromuscular junction. Nat. Protoc. 2: 1117–1125. https://doi.org/10.1038/nprot.2007.142

Lloyd, T. E., J. Machamer, K. O'Hara, J. H. Kim, S. E. Collins *et al.*, 2012 The p150(Glued) CAP-Gly domain regulates initiation of retrograde transport at synaptic termini. Neuron 74: 344–360. https://doi.org/10.1016/j.neuron.2012.02.026

Marchesin, V., A. Castro-Castro, C. Lodillinsky, A. Castagnino, J. Cyrta *et al.*, 2015 ARF6–JIP3/4 regulate endosomal tubules for MT1-MMP exocytosis in cancer invasion. J. Cell Biol. 211: 339–358. https://doi.org/10.1083/jcb.201506002

Marie, B., S. T. Sweeney, K. E. Poskanzer, J. Roos, R. B. Kelly *et al.*, 2004 Dap160/intersectin scaffolds the periactive zone to achieve high-fidelity endocytosis and normal synaptic growth. Neuron 43: 207–219. https://doi.org/10.1016/j.neuron.2004.07.001

Marqués, G., H. Bao, T. E. Haerry, M. J. Shimell, P. Duchek *et al.*, 2002 The *Drosophila* BMP type II receptor Wishful Thinking regulates neuromuscular synapse morphology and function. Neuron 33: 529–543. https://doi.org/10.1016/S0896-6273(02)00595-0

Marrus, S. B., S. L. Portman, M. J. Allen, K. G. Moffat, and A. DiAntonio, 2004 Differential localization of glutamate receptor subunits at the *Drosophila* neuromuscular junction. J. Neurosci. 24: 1406–1415. https://doi.org/10.1523/JNEUROSCI.1575-03.2004

McCabe, B. D., G. Marqués, A. P. Haghighi, R. D. Fetter, M. L. Crotty *et al.*, 2003 The BMP homolog Gbb provides a retrograde signal that regulates synaptic growth at the *Drosophila* neuromuscular junction. Neuron 39: 241–254. https://doi.org/10.1016/S0896-6273(03)00426-4

McCabe, B. D., S. Hom, H. Aberle, R. D. Fetter, G. Marqués *et al.*, 2004 Highwire regulates presynaptic BMP signaling essential for synaptic growth. Neuron 41: 891–905. https://doi.org/10.1016/S0896-6273(04)00073-X

McKenney, R. J., W. Huynh, M. E. Tanenbaum, G. Bhabha, and R. D. Vale, 2014 Activation of cytoplasmic dynein motility by dynactin-cargo adapter complexes. Science 345: 337–341. https://doi.org/10.1126/science.1254198

Montagnac, G., J. B. Sibarita, S. Loubéry, L. Daviet, M. Romao *et al.*, 2009 ARF6 Interacts with JIP4 to control a motor switch mechanism regulating endosome traffic in cytokinesis. Curr. Biol. 19: 184–195. https://doi.org/10.1016/j.cub.2008.12.043

Moughamian, A. J., and E. L. Holzbaur, 2012 Dynactin is required for transport initiation from the distal axon. Neuron 74: 331–343. https://doi.org/10.1016/j.neuron.2012.02.025

Moughamian, A. J., G. E. Osborn, J. E. Lazarus, S. Maday, and E. L. F. Holzbaur, 2013 Ordered recruitment of dynactin to

the microtubule plus-end is required for efficient initiation of retrograde axonal transport. J. Neurosci. 33: 13190–13203. https://doi.org/10.1523/JNEUROSCI.0935-13.2013

Narayanan, R., H. Krämer, and M. Ramaswami, 2000 *Drosophila* endosomal proteins hook and deep orange regulate synapse size but not synaptic vesicle recycling. J. Neurobiol. 45: 105–119. https://doi.org/10.1002/1097-4695(20001105)45:2<105::AID-NEU5>3.0.CO;2-X

Neisch, A. L., A. W. Avery, J. B. Machamer, M. G. Li, and T. S. Hays, 2016 Methods to identify and analyze gene products involved in neuronal intracellular transport using *Drosophila*. Methods Cell Biol. 131: 277–309. https://doi.org/10.1016/bs.mcb.2015.06.015

Obholzer, N., S. Wolfson, J. G. Trapani, W. Mo, A. Nechiporuk *et al.*, 2008 Vesicular glutamate transporter 3 is required for synaptic transmission in zebrafish hair cells. J. Neurosci. 28: 2110–2118. https://doi.org/10.1523/JNEUROSCI.5230-07.2008

O'Connor-Giles, K. M., L. L. Ho, and B. Ganetzky, 2008 Nervous wreck interacts with thickveins and the endocytic machinery to attenuate retrograde BMP signaling during synaptic growth. Neuron 58: 507–518. https://doi.org/10.1016/j.neuron.2008.03.007

Persson, U., H. Izumi, S. Souchelnytskyi, S. Itoh, S. Grimsby *et al.*, 1998 The L45 loop in type I receptors for TGF-beta family members is a critical determinant in specifying Smad isoform activation. FEBS Lett. 434: 83–87. https://doi.org/10.1016/S0014-5793(98)00954-5

Rao, S., C. Lang, E. S. Levitan, and D. L. Deitcher, 2001 Visualization of neuropeptide expression, transport, and exocytosis in *Drosophila melanogaster*. J. Neurobiol. 49: 159–172. https://doi.org/10.1002/neu.1072

Rawson, J. M., M. Lee, E. L. Kennedy, and S. B. Selleck, 2003 *Drosophila* neuromuscular synapse assembly and function require the TGF-beta type I receptor saxophone and the transcription factor Mad. J. Neurobiol. 55: 134–150. https://doi.org/10.1002/neu.10189

Reck-Peterson, S. L., W. B. Redwine, R. D. Vale, and A. P. Carter, 2018 The cytoplasmic dynein transport machinery and its many cargoes. Nat. Rev. Mol. Cell Biol. 19: 382–398 (erratum: Nat. Rev. Mol. Cell Biol. 19: 479). https://doi.org/10.1038/s41580-018-0004-3

Roy, S., H. Huang, S. Liu, and T. B. Kornberg, 2014 Cytoneme-mediated contact-dependent transport of the *Drosophila* decapentaplegic signaling protein. Science 343: 1244624. https://doi.org/10.1126/science.1244624

Sanda, M., N. Ohara, A. Kamata, Y. Hara, H. Tamaki *et al.*, 2010 Vezatin, a potential target for ADP-ribosylation factor 6, regulates the dendritic formation of hippocampal neurons. Neurosci. Res. 67: 126–136. https://doi.org/10.1016/j.neures.2010.02.008

Schindelin, J., I. Arganda-Carreras, E. Frise, V. Kaynig, M. Longair *et al.*, 2012 Fiji: an open-source platform for biological-image analysis. Nat. Methods 9: 676–682. https://doi.org/10.1038/nmeth.2019

Schlager M. A., H. T. Hoang, L. Urnavicius, S. L. Bullock, and A. P. Carter, 2014 In vitro reconstitution of a highly processive recombinant human dynein complex. EMBO J. 33: 1855–1868. https://doi.org/10.15252/embj.201488792

Smith, R. B., J. B. Machamer, N. C. Kim, T. S. Hays, and G. Marqués, 2012 Relay of retrograde synaptogenic signals through axonal transport of BMP receptors. J. Cell Sci. 125: 3752–3764. https://doi.org/10.1242/jcs.094292

Sulkowski, M. J., T. H. Han, C. Ott, Q. Wang, E. M. Verheyen *et al.*, 2016 A novel, noncanonical BMP pathway modulates synapse maturation at the *Drosophila* neuromuscular junction. PLoS Genet. 12: e1005810 [corrigenda: PLoS Genet. 14: e1007343 (2018)]. https://doi.org/10.1371/journal.pgen.1005810

Sunio, A., A. B. Metcalf, and H. Krämer, 1999 Genetic dissection of endocytic trafficking in *Drosophila* using a horseradish peroxidase-bride of sevenless chimera: hook is required for normal maturation of multivesicular endosomes. Mol. Biol. Cell 10: 847–859. https://doi.org/10.1091/mbc.10.4.847

Szatmári, Z., V. Kis, M. Lippai, K. Hegedus, T. Faragó *et al.*, 2014 Rab11 facilitates cross-talk between autophagy and endosomal pathway through regulation of Hook localization. Mol. Biol. Cell 25: 522–531. https://doi.org/10.1091/mbc.e13-10-0574

Urnavicius, L., C. K. Lau, M. M. Elshenawy, E. Morales-Rios, C. Motz *et al.*, 2018 Cryo-EM shows how dynactin recruits two dyneins for faster movement. Nature 554: 202–206. https://doi.org/10.1038/nature25462

Wang, J. W., E. S. Beck, and B. D. McCabe, 2012 A modular toolset for recombination transgenesis and neurogenetic analysis of *Drosophila*. PLoS One 7: e42102. https://doi.org/10.1371/journal.pone.0042102

Westerfield, M., 1993 *The Zebrafish Book: A Guide for the Laboratory Use of zebrafish (Brachydanio rerio)*, University of Oregon Press, Eugene, OR.

Williamson, C. D., and J. G. Donaldson, 2019 Arf6, JIP3, and dynein shape and mediate macropinocytosis. Mol. Biol. Cell 30: 1477–1489. https://doi.org/10.1091/mbc.E19-01-0022

Wong, M. Y., C. Zhou, D. Shakiryanova, T. E. Lloyd, D. L. Deitcher *et al.*, 2012 Neuropeptide delivery to synapses by long-range vesicle circulation and sporadic capture. Cell 148: 1029–1038. https://doi.org/10.1016/j.cell.2011.12.036

Xiang, X., R. Qiu, X. Yao, H. N. Arst, Jr., M. A. Peñalva *et al.*, 2015 Cytoplasmic dynein and early endosome transport. Cell. Mol. Life Sci. 72: 3267–3280. https://doi.org/10.1007/s00018-015-1926-y

Yao, X., H. N. Arst, Jr., X. Wang, and X. Xiang, 2015 Discovery of a vezatin-like protein for dynein-mediated early endosome transport. Mol. Biol. Cell 26: 3816–3827. https://doi.org/10.1091/mbc.E15-08-0602

Communicating editor: K. O'Connor-Giles